Dual-Controlled Macroscopic Motions in A Supramolecular Hierarchical Assembly of Motor Amphiphiles

Leung, Franco King-Chi; Kajitani, Takashi; Stuart, Marc C. A.; Fukushima, Takanori; Feringa, Ben L.

Published in:
Angewandte Chemie (International ed. in English)

DOI:
10.1002/anie.201905445

Publication date:
2019

A Journal of the Gesellschaft Deutscher Chemiker

Angewandte International Edition Chemie

GDCh

www.angewandte.org

Accepted Article

Title: Dual-Controlled Macroscopic Motions in A Supramolecular Hierarchical Assembly of Motor Amphiphiles

Authors: Ben Lucas Feringa, Franco King-Chi Leung, Marc C. A. Stuart, Takashi Kajitani, and Takanori Fukushima

To be cited as: *Angew. Chem. Int. Ed.* 10.1002/anie.201905445
Angew. Chem. 10.1002/ange.201905445

Link to VoR: http://dx.doi.org/10.1002/anie.201905445
http://dx.doi.org/10.1002/ange.201905445

WILEY-VCH

10.1002/anie.201905445

WILEY-VCH

Dual-Controlled Macroscopic Motions in A Supramolecular Hierarchical Assembly of Motor Amphiphiles

Franco King-Chi Leung,*[a] Takashi Kajitani,[b] Marc C. A. Stuart,[a] Takanori Fukushima,[b] and Ben L. Feringa*[a]

Abstract: Three-dimensional unidirectionally aligned and responsive supramolecular hierarchical assemblies have much potential in adaptive materials for biomedical and soft actuator applications. However, to achieve systematical control of the motion of stimuli-responsive materials by orthogonal external stimuli and to complete a series of complicated tasks remains a grand challenge. Herein, we demonstrate a novel designed hybrid supramolecular assembly of molecular motor amphiphiles that also serves as a template for iron nanoparticles growth, and as a consequence this soft hybrid material is orthogonally controlled by dual light/magnetic stimuli. Macroscopic motor amphiphile strings, decorated with iron nanoparticles, provide fast response photoactuations and magnet induced movements that allows a precisely controlled cargo transport process.

Functional supramolecular polymers found in living systems are playing vital roles in key biological functions magnificent expressed in controlled transport and movement.[1–4] While biological systems allow precisely controlled supramolecular polymerization, synthetic supramolecular polymers[5–7] were implemented with functional tunability and stimuli responsiveness features by delicate organic molecular design.[6–15] This strategy allows the construction of hierarchical supramolecular systems to provide various man-made stimuli-responsive functions along multiple length-scales. At microscopic length-scale,[11,12] numerous amphiphilic molecules have been shown to assemble into one-dimensional (1D) supramolecular polymers allowing various functions,[16,17] *e.g.,* morphological transformation[18–27] and control of cell growth.[18,28,29] Furthermore, it has been demonstrated that these 1D supramolecular polymers can be controlled by external stimuli, for instance, light,[22] heat,[18,30] pH,[23,25,27–29] small organic molecules,[20,26] and ions.[19,21] Some of the 1D supramolecular polymers can be controlled by various external stimuli simultaneously,[24,31] allowing orthogonal control of supramolecular polymers functions. At macroscopic length-scales, the obtained 1D supramolecular polymers of unimolecular amphiphiles can further assemble into randomly entangled 3D networks, alternatively, 3D unidirectionally aligned hierarchical supramolecular structures generate exciting opportunities towards applications in regenerative biomedical materials,[32–34] anisotropic actuators,[35,36] electronic and optoelectronic materials.[37–39] We recently demonstrated the first photo-controlled unidirectionally aligned hierarchical supramolecular structure in aqueous media to realize a photo-controlled macroscopic muscle-type actuation in both water and air.[36] This small molecule supramolecular approach provides a complementary method to existing macroscopic actuators obtained by stimuli-responsive crystals,[40–43] polymeric gel,[44–47] and polymeric liquid crystals.[48–54] Noticeably, the orientational structural order of the macroscopic string of motor amphiphiles (MA) could be fine adjusted by the electrostatic interaction between carboxylate groups of MA and counter-ions, *e.g.,* Ca^{2+} and Mg^{2+}, allowing a precise control of actuation speed by non-invasive photoirradiation.[55] The large anisotropic morphological transformation of a MA string could potentially provide novel strategies for various macroscopic soft robotic tasks, including cargo carrier and weight lifting, which remains highly challenging for isotropic motions of the randomly entangled 3D supramolecular networks. To exert the full potential of the unidirectionally aligned hierarchical supramolecular structure of MA, an alternative non-invasive external stimulus, functioning orthogonally with light, is urgently needed for developing more sophisticated macroscopic motion processes based on a MA string. However, to the best of our knowledge, dual controlled macroscopic functions of a unidirectionally aligned hierarchical supramolecular structure has remained unexplored.

Herein, we demonstrate a dual light/magnetic field controlled hybrid supramolecular material by the templating growth of magnetite nanoparticles (Fe_3O_4) onto molecular motor based supramolecular nanofibers of MAs. The MA nanofibers decorated with iron nano-particles (FeNP) are assembled by a shear flow method in a $CaCl_2$ solution to afford 3D-assembled macroscopic string. The macroscopic string of MA is actuated/moved upon photo-irradiation while placed closely to a permanent magnet. Stupp *et al.* have demonstrated that the histidine functionalized peptide amphiphilic nanofibers serve as a template of Fe_3O_4 nanoparticles to control the morphology and size uniformity of the FeNP.[56] The $\mathbf{MA_{His}}$ was designed with the second-generation molecular motor attached with a dodecyl chain to the upper half and two histidine moieties were connected with alkyl-linkers as the lower half of the motor (Figure 1). Fe^{2+} and Fe^{3+} ions serve as precursors of the Fe_3O_4 formation by binding to the imidazole motifs of histidine and the terminal carboxylic acid groups of $\mathbf{MA_{His}}$. By elucidation of the key design principles of the supramolecular muscle, this could open up new prospects towards the development of dual stimuli-controlled supramolecular materials and future soft robotic systems.

[a] Dr. F. K. C. Leung, Dr. M. A. C. Stuart and Prof. Dr. B. L. Feringa
Stratingh Institute for Chemistry, University of Groningen
Nijenborgh 4, 9747AG Groningen (Netherlands)
E-mail: k.c.leung@rug.nl, b.l.feringa@rug.nl
[b] Dr. T. Kajitani and Prof. Dr. T. Fukushima
Laboratory for Chemistry and Life Science, Institute of Innovative Research, Tokyo Institute of Technology
4259 Nagatsuta, Midori-ku, Yokohama 226-8503 (Japan)

Supporting information for this article is given via a link at the end of the document.((Please delete this text if not appropriate))

10.1002/anie.201905445

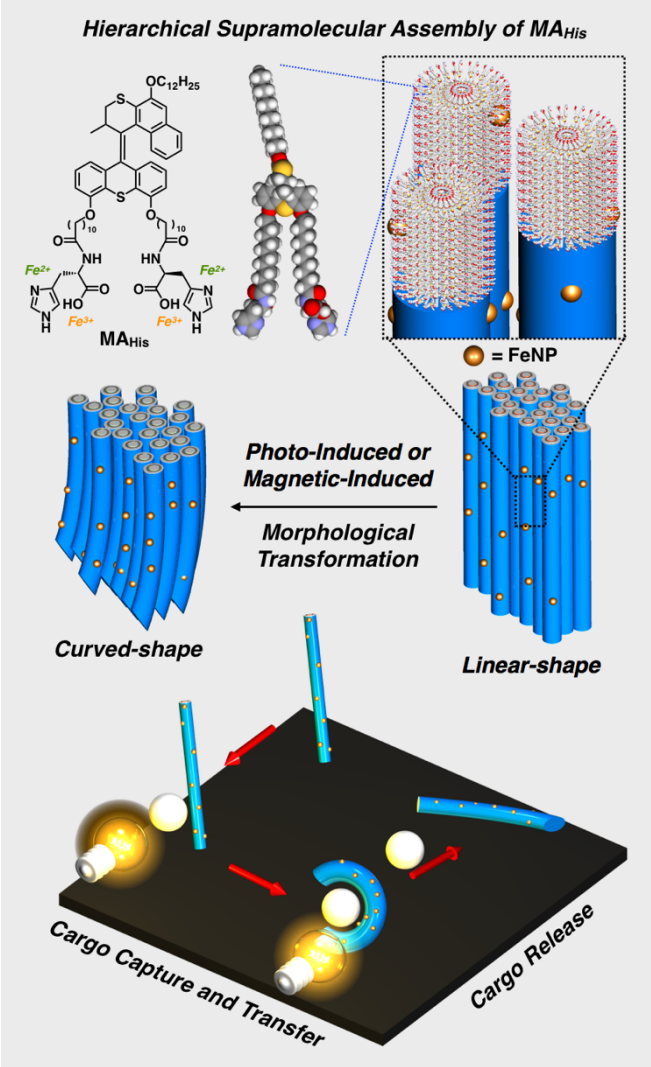

Figure 1. Schematic illustration of the molecular structure of molecular motor amphiphile (**MA$_{His}$**), the hierarchical organization and photoactuation and magnetic field induced motions of the assembled structures in the obtained macroscopic string.

The synthesis, characterization and photoisomerization processes of **MA$_{His}$** are summarized in the Supporting Information (Figures S11–16). The **MA$_{His}$** (5.0 wt.%, 39.5 mM) was dissolved in double deionized water at 25 °C. A Nile Red fluorescence assay (NRFA), which probes the internal hydrophobicity of assembly, revealed a decrease in blue shift when diluting beyond 0.01 mM of **MA$_{His}$** and showed a critical aggregation concentration (CAC) of 3.15 μM (Figure S1). This freshly prepared solution of **MA$_{His}$** diluted into 0.5 wt.% (3.95 mM, above CAC) was imaged using cryogenic transmission electron microscopy (cryo-TEM) revealing that **MA$_{His}$** assembled into short fibers (50~100 nm in length) and about 7 to 8 nm in diameter (Figure S2a), while no significant change was observed after 1 week aging of the identical sample (Figure S2b). Interestingly, these fibers grew longitudinally into hundreds of nanometers to micrometers in length after 4 weeks aging in the identical medium, while the diameter remained unchanged (Figures 2a). Subsequent mineralization of **MA$_{His}$** nanofibers (6.3 μL, 39.5 mM), using $FeCl_2$:$FeCl_3$ (1:2, 5.0 μL, 100 mM), was performed to yield a pale yellow solution after exposure to ammonia vapors for 30 min at 25 °C to afford **MA$_{His/FeNP}$** without disruption of fibers integrity (Figures 2b). Notably, most of the particles (~3 nm in size) formed in direct contact with the **MA$_{His}$** nanofibers surface. The presence of these small particles at the nanofibers suggested that nucleation and growth may take place on the fiber surface instead of in solution.[56] However, mineralization of **MA$_{C10}$** nanofibers (Figure S3), performed by the identical method, has shown that less particles are in direct contact with the fibers than those of in the mineralized sample of **MA$_{His/FeNP}$** (Figure 2b). The results indicated that the imidazole and carboxylic acid moieties of histidine play key roles in Fe_3O_4 nanoparticles nucleation and growth on the **MA$_{His}$** nanofiber surface.

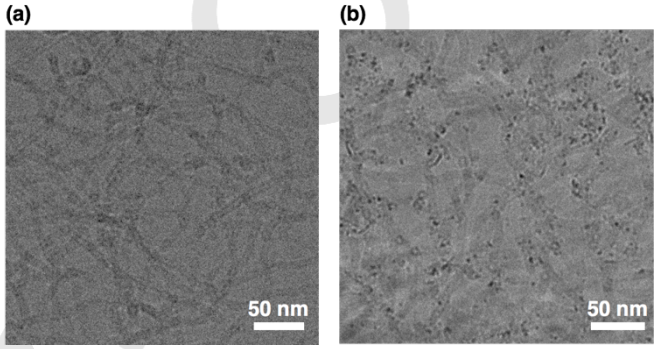

Figure 2. (a) Cryo-TEM images of **MA$_{His}$** (3.95 mM, above CAC) aged for 4 weeks. (b) Cryo-TEM image of **MA$_{His}$** nanofibers aged for 4 weeks (6.3 μL, 39.5 mM) was added with $FeCl_2$:$FeCl_3$ (1:2, 5.0 μL, 100 mM) and then exposed to ammonia vapors for 30 min at 25 °C to afford **MA$_{His/FeNP}$** that diluted to 3.95 mM as final concentration.

With the FeNP decorated **MA$_{His}$** nanofibers (**MA$_{His/FeNP}$**), this hybrid supramolecular polymer was assembled into macroscopic length-scale hierarchical structure by applying a shear flow method in aq. $CaCl_2$ solution (150 mM). This weak macroscopic string showed no unidirectional alignment in scanning electron microscopy (SEM) and polarized optical microscopy (POM) measurements (Figure S4a and S4b). Meanwhile, a macroscopic string prepared from **MA$_{His}$** solution (5.0 wt.%, 39.5 mM) showed weak alignment in POM and SEM measurements (Figure S5a and S5b). To provide structural parameters and orientation order of **MA$_{His}$** nanofibers in the macroscopic string, through-view small-angle X-ray scattering (SAXS) measurements were performed. In the 2D SAXS image of the **MA$_{His}$** string prepared from $CaCl_2$ solution on a sapphire substrate at 25 °C (Figure S5c), a pair of weak spot-like scatterings was observed in a smaller-angle region (q = 0.1–0.45 nm^{-1}) (Figure S5c, inset), which is due to scattering from the unidirectionally aligned nanofiber bundles of **MA$_{His}$**. The diffraction arc with d-spacing of 6.39 nm (Figure S5d), arising from the diffraction from the (001) plane of a lamellar structure, while the string prepared from **MA$_{His/FeNP}$** showed no scattering and alignment in the measurement (Figure S4c and S4d). The results indicated that carboxylic acid groups of **MA$_{His}$** have been occupied in mineralization with ferric ions to prohibit further alignment of **MA$_{His/FeNP}$** nanofibers by the shear flow method in a $CaCl_2$ solution.

To improve the orientation order and mechanical stability of **MA$_{His/FeNP}$** macroscopic nanofibers, **MA$_{C10}$** nanofibers were blended into **MA$_{His/FeNP}$** nanofibers, which showed a higher

structural and orientation order than that of **MA$_{His}$** nanofibers observed in SAXS measurements. The freshly prepared **MA$_{His/FeNP}$** nanofibers blended with **MA$_{C10}$** nanofibers (molar ratio: 1:2) was ejected into a swallow pool of $CaCl_2$ solution (150 mM) on a sapphire substrate at 25 °C to afford a stable macroscopic string. The string showed uniform birefringence in the direction of the string long axis in POM images (Figures 3a and S6). Notably, no iron nanoparticles exchange between nanofibers of **MA$_{His/FeNP}$** and **MA$_{C10}$** was observed by cryo-TEM (Figure S7). SEM images of the string showed arrays of unidirectionally aligned nanofiber bundles (Figure 3b). The POM and SEM images are essentially identical to that of observed in the string prepared form **MA$_{His}$:MA$_{C10}$** (molar ratio 1:2) (Figure S8a and S8b). In the 2D-SAXS image of **MA$_{His/FeNP}$:MA$_{C10}$** string, a pair of spot-like scatterings was observed in a smaller-angle region (q = 0.1–0.45 nm^{-1}) (Figure 3c, inset), which is due to scatterings from the unidirectionally aligned nanofiber bundles of **MA$_{His/FeNP}$:MA$_{C10}$**. The diffraction arc with d-spacing of 6.19 nm oriented from the diffraction of (001) plane of a lamellar structure, indicating that the degree of alignment in the blend string was improved (Figure 3d) compared to that observed in the string of **MA$_{His}$** (Figure S5c and S5d). It should be noted that a structural disordering was observed in the lamellar structure of string of **MA$_{His/FeNP}$:MA$_{C10}$** (Figure 3c and 3d) in comparison to the lamellar structure of string of **MA$_{His}$:MA$_{C10}$** (Figure S8c and S8d), however the muscle function can still be achieved (*vide infra*).

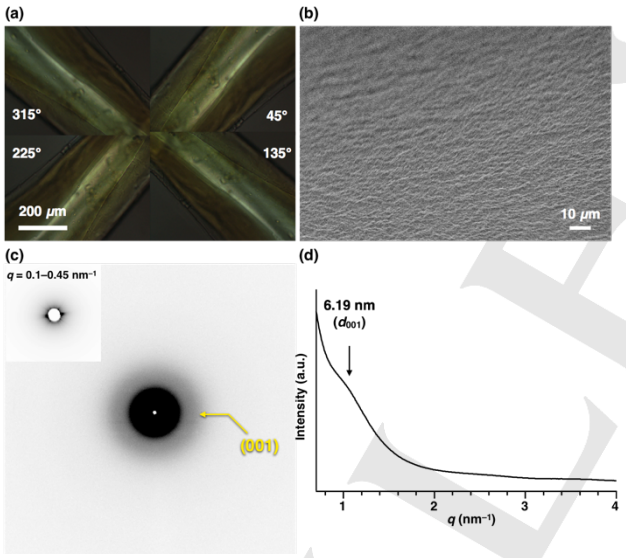

Figure 3. (a) POM images of a macroscopic aligned string composed of **MA$_{His/FeNP}$:MA$_{C10}$** (molar ratio 1:2) prepared from aq. solutions of $CaCl_2$ (150 mM) under crossed polarizers. The POM images of the string were tilted at 45°, 135°, 225°, and 315° relative to the transmission axis of the analyzer. Scale bar for all panels. (b) SEM and (c) 2D SAXS images of a macroscopic aligned string composed of **MA$_{His/FeNP}$:MA$_{C10}$** (molar ratio 1:2) (inset: enlarged 2D image for q = 0.1–0.45 nm^{-1} at 25 °C. (d) 1D SAXS patterns of a macroscopic aligned string composed of **MA$_{His/FeNP}$:MA$_{C10}$** (molar ratio 1:2) of 2D SAXS images in (c), showing the diffraction pattern in the direction perpendicular to long axis of the string.

Upon photoirradiation (λ = 365 nm), the **MA$_{His/FeNP}$:MA$_{C10}$** string bent towards the light source from initial angle of 0° to a saturated flexion angle of 90° within 25 s, which is proof of large amplitude actuation of the hybridized soft material (Figure S9 and Movie S1). To investigate the structural changes during photoactuation of the **MA$_{His/FeNP}$:MA$_{C10}$** string, we carried out *in-situ* SAXS measurements (Figures 4, S10, and Movie S2). Upon exposure to the X-ray beam, the string gave a diffraction pattern (Figures 4a and S10a) which is essentially identical to that of observed for a string on a sapphire (Figure 3c and 3d). Following UV light irradiation for 60 s in total, the string bent by 25° towards the incident light source (Figure 4b, inset). The 1D-diffraction pattern showed that the d-spacing of the diffraction from the (001) plane was increased from 6.21 to 6.33 nm in the resulting SAXS pattern (Figures 4b and S10d). The increase in the d-spacing due to the diffraction of the (001) plane indicates that this photoactuation process is accompanied by an increase in the diameter of the nanofibers. Furthermore, the pair of spot-like scatterings in a smaller-angle region (q = 0.1–0.45 nm^{-1}), which is initially observed in the horizontal direction (Figure S10e–S10h), started to rotate in response to UV light, resulting in a tilt angle of 25° after 60 s irradiation in total, where the string bent by 25° (Figure 4b, inset). This consistency between tilt angle of the scatterings and the bending angle of the string indicates that the macroscopic bending of the string is caused by orientational changes of the unidirectionally aligned nanofiber bundles.

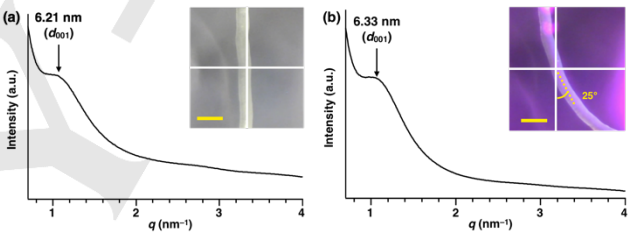

Figure 4. 1D SAXS patterns and photographs (inset scale bars, 500 μm) of a string suspended in air after UV irradiation at 25 °C for (a) 0 s and (d) 60 s. Intersections of the two white lines in the photographs represent the centre of the X-ray beam. Values in parentheses in the 1D SAXS patterns indicate Miller indices.

When a magnet was placed close to the **MA$_{His/FeNP}$:MA$_{C10}$** string, a bending motion towards the magnet was observed within 2 s, indicating that the **MA$_{His/FeNP}$:MA$_{C10}$** string can also be controlled by magnetic stimulus (Figure 5a and Movie S3). To provide a dual controlled process of the **MA$_{His/FeNP}$:MA$_{C10}$** string, a cargo transport experiment was carried out (Figure 5 and Movie S4). A **MA$_{His/FeNP}$:MA$_{C10}$** string was prepared and placed at position A in the pool of aq. $CaCl_2$ solution (150 mM, Figure 5b), while a piece of paper has placed at position B. A magnet was employed to guide the **MA$_{His/FeNP}$:MA$_{C10}$** string moving from position A to B (Figure 5c). Upon photoirradiation (λ = 365 nm), the **MA$_{His/FeNP}$:MA$_{C10}$** string started to change from a linear-shape to a curved-shape within 60 s, which the light source is ~ 1 cm away from the **MA$_{His/FeNP}$:MA$_{C10}$** string (Figure 5d). The curved-shape **MA$_{His/FeNP}$:MA$_{C10}$** string was carrying the piece of paper to move from position B to C, and this process was guided by the magnet (Figure 5e) When the back-side of curved-shape **MA$_{His/FeNP}$:MA$_{C10}$** string was irradiated (λ = 365 nm), it transformed from curved-shape to linear-shape inducing the unloading process at position C (Figure 5f). Finally, the linear-shape **MA$_{His/FeNP}$:MA$_{C10}$** string was guided to position D (Figure 5g). This experiment successfully demonstrated the **MA$_{His/FeNP}$:MA$_{C10}$** string was controlled orthogonally by light and magnet stimuli to perform a cargo transport process macroscopically.

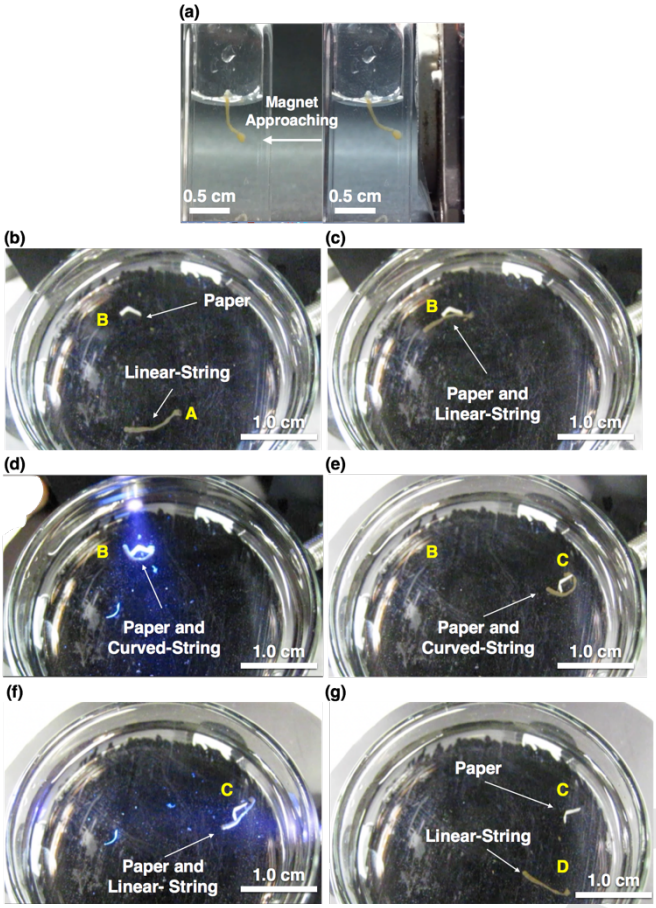

Figure 5. (a) Snapshots of a $\mathbf{MA_{His/FeNP}}$:$\mathbf{MA_{C10}}$ string in $CaCl_2$ solution (150 mM) bends towards a magnet from the right. Snapshots of a dual-controlled cargo process in $CaCl_2$ solution (150 mM) (b) $\mathbf{MA_{His/FeNP}}$:$\mathbf{MA_{C10}}$ string (Position A) and paper (Position B), (c) the string moved toward position B, (d) the string changed to a curved-shape upon photoirradiation, (e) the paper was carried to position C by the string which guided by a magnet, (f) the string changed to a linear-shape upon photoirradiation, (g) the paper was unloaded and the string moved to position D.

In summary, motor amphiphiles functionalized with the histidine moieties at the lower half of the motor motif were synthesized and probed for hierarchical assembly and dynamic properties. Nanofibers of $\mathbf{MA_{His}}$ and FeNP decorated nanofibers of $\mathbf{MA_{His/FeNP}}$ in water were observed. By applying a shear flow method, macroscopic strings of $\mathbf{MA_{His}}$ and $\mathbf{MA_{His/FeNP}}$:$\mathbf{MA_{C10}}$ prepared from calcium chloride solution provided a unidirectional alignment which facilitated a fast response to light during photoactuation. Furthermore, the macroscopic string of $\mathbf{MA_{His/FeNP}}$:$\mathbf{MA_{C10}}$ was controlled by a magnet to show macroscopic movements and applied for a cargo transport process to perform a load/unload and translocation actions. The current approach demonstrates the potential of generating muscle-like function and cargo transport by dual stimuli controlled events and opens a new direction for generating future soft robotic materials.

Acknowledgements

This work was supported financially by the Croucher Foundation (Croucher Postdoctoral Fellowship to F.K.C.L), the Netherlands Organization for Scientific Research (NWO-CW), the European Research Council (ERC; advanced grant no. 694345 to B.L.F.), the Ministry of Education, Culture and Science (Gravitation program no. 024.001.035), and a Grant-in-Aid for Scientific Research on Innovative Areas “π-Figuration” (no. 26102008 and no. 15K21721) of The Ministry of Education, Culture, Sports, Science and Technology (MEXT), Japan. The synchrotron XRD experiments were performed at the BL45XU in the SPring-8 with the approval of the RIKEN SPring-8 Center (proposal no. 20160027).

Keywords: Hierarchical Supramolecular Polymer • Molecular Motor • Macroscopic Actuation • Dual-Control • Soft Materials

[1] N. S. Simmons, E. R. Blout, *Biophys. J.* **1960**, *1*, 55–62.
[2] T. Lino, *J. Supramol. Struct.* **1974**, *2*, 372–384.
[3] D. S. Goodsell, *The Machinery of Life*. (**1993**). New York: Springer-Verlag.
[4] H. Hess *Annu. Rev. Biomed. Eng.* **2011**, *13*, 429–450.
[5] J. M. Lehn, *Polym. Int.* **2002**, *51*, 825–839.
[6] G. V. Oshovsky, D. N. Reinhoudt, W. Verboom, *Angew. Chem. Int. Ed.* **2007**, *46*, 2366–2393.
[7] R. J. Wojtecki, M. A. Meador, S. J. Rowan, *Nat. Mater.* **2011**, *10*, 14–27.
[8] A. Mulder, J. Huskens, D. N. Reinhoudt, *Org. Biomol. Chem.* **2004**, *2*, 3409–3424.
[9] L. C. Palmer, S. I. Stupp, *Acc. Chem. Res.* **2008**, *41*, 1674–1684.
[10] T. F. A. de Greef, E. W. Meijer, *Nature* **2008**, *453*, 171–173.
[11] E. Krieg, B. Rybtchinski, *Chem. - A Eur. J.* **2011**, *17*, 9016–9026.
[12] S. L. Li, T. Xiao, C. Lin, L. Wang, *Chem. Soc. Rev.* **2012**, *41*, 5950–5968.
[13] X. Yan, F. Wang, B. Zheng, F. Huang, *Chem. Soc. Rev.* **2012**, *41*, 6042–6065.
[14] T. Aida, E. W. Meijer, S. I. Stupp, *Science* **2012**, *335*, 813–817.
[15] R. Dong, Y. Zhou, X. Huang, X. Zhu, Y. Lu, J. Shen, *Adv. Mater.* **2015**, *27*, 498–526.
[16] D. W. P. M. Lowik, E. H. P. Leunissen, M. van den Heuvel, M. B. Hansen, J. C. M. van Hest, *Chem. Soc. Rev.* **2010**, *39*, 3394–3412.
[17] E. Krieg, M. M. C. Bastings, P. Besenius, B. Rybtchinski, *Chem. Rev.* **2016**, *116*, 2414–2477.
[18] Z. Huang, H. Lee, E. Lee, S. Kang, J. Nam, M. Lee, *Nat. Commun.* **2011**, *2*, 455–459.
[19] H. Kim, S. Kang, Y. Lee, C. Seok, J. Lee, W. Zin, M. Lee, *Angew. Chem. Int. Ed.* **2010**, *49*, 8471–8475.
[20] Y. Wang, Z. Huang, Y. Kim, Y. He, M. Lee, *J. Am. Chem. Soc.* **2014**, *136*, 16152–16155.
[21] S. Shin, S. Lim, Y. Kim, T. Kim, T. Choi, M. Lee, *J. Am. Chem. Soc.* **2013**, *135*, 2156–2159.
[22] P. Kuad, A. Miyawaki, Y. Takashima, H. Yamaguchi, A. Harada, *J. Am. Chem. Soc.* **2007**, *129*, 12630–12631.
[23] H. Frisch, Y. Nie, S. Raunser, P. Besenius, *Chem. - A Eur. J.* **2015**, *21*, 3304–3309.
[24] H. A. M. Ardona, J. D. Tovar, *Chem. Sci.* **2015**, *6*, 1474–1484.
[25] A. Dehsorkhi, V. Castelletto, I. W. Hamley, J. Adamcik, R. Mezzenga, *Soft Matter* **2013**, *9*, 6033–6036.
[26] Z. Huang, S.-K. Kang, M. Lee, *J. Mater. Chem.* **2011**, *21*, 15327–15331.
[27] J. Zhang, R. Hao, L. Huang, J. Yao, X. Chen, Z. Shao, *Chem. Commun.* **2011**, *47*, 10296–10298.
[28] T. J. Moyer, J. A. Finbloom, F. Chen, D. J. Toft, V. L. Cryns, S. I. Stupp, *J. Am. Chem. Soc.* **2014**, *136*, 14746–14752.
[29] B. F. Lin, K. A. Megley, N. Viswanathan, D. V. Krogstad, L. B. Drews, M. J. Kade, M. V Tirrell, *J. Mater. Chem.* **2012**, *22*, 19447–19454.
[30] S. Zhang, M. A. Greenfield, A. Mata, L. C. Palmer, R. Bitton, J. R. Mantei, C. Aparicio, M. Olvera de la Cruz, S. I. Stupp, *Nat. Mater.* **2010**, *9*, 594–601.
[31] M. von Groning, I. de Feijte, M. C. A. Stuart, I. K. Voets, P. Besenius, *J. Mater. Chem. B* **2013**, *1*, 2008–2012.
[32] J. B. Matson, S. I. Stupp, *Chem. Commun.* **2012**, *48*, 26–33.
[33] S. I. Stupp, R. H. Zha, L. C. Palmer, H. Cui, R. Bitton, *Faraday Discuss.* **2013**, *166*, 9–30.
[34] M. J. Webber, E. J. Berns, S. I. Stupp, *Isr. J. Chem.* **2013**, *53*, 530–554.
[35] S. M. Chin, C. V Synatschke, S. Liu, R. J. Nap, N. A. Sather, Q. Wang, Z. Álvarez, A. N. Edelbrock, T. Fyrner, L. C. Palmer, I. Szleifer, M. Olvera de la Cruz, S.I. Stupp., *Nat. Commun.* **2018**, *9*,

2395.
[36] J. Chen, F. K. C. Leung, M. C. A. Stuart, T. Kajitani, T. Fukushima, E. van der Giessen, B. L. Feringa, *Nat. Chem.* **2018**, *10*, 132–138.
[37] B. D. Wall, S. R. Diegelmann, S. Zhang, T. J. Dawidczyk, W. L. Wilson, H. E. Katz, H. Q. Mao, J. D. Tovar, *Adv. Mater.* **2011**, *23*, 5009–5014.
[38] K. Besar, H. A. M. Ardoña, J. D. Tovar, H. E. Katz, *ACS Nano* **2015**, *9*, 12401–12409.
[39] A. M. Sanders, T. J. Magnanelli, A. E. Bragg, J. D. Tovar, *J. Am. Chem. Soc.* **2016**, *138*, 3362–3370.
[40] D. Kitagawa, H. Nishi, S. Kobatake, *Angew. Chem. Int. Ed.* **2013**, *52*, 9320–9322.
[41] M. Irie, T. Fukaminato, K. Matsuda, S. Kobatake, *Chem. Rev.* **2014**, *114*, 12174–12277.
[42] M. Morimoto, M. Irie, *J. Am. Chem. Soc.* **2010**, *132*, 14172–14178.
[43] T. Ikegami, Y. Kageyama, K. Obara, S. Takeda, *Angew. Chem. Int. Ed.* **2016**, *55*, 8239–8243.
[44] A. Harada, Y. Takashima, M. Nakahata, *Acc. Chem. Res.* **2014**, *47*, 2128–2140.
[45] Q. Li, G. Fuks, E. Moulin, M. Maaloum, M. Rawiso, I. Kulic, J. T. Foy, N. Giuseppone, *Nat. Nanotechnol.* **2015**, *10*, 161–165.
[46] K. Iwaso, Y. Takashima, A. Harada, *Nat. Chem.* **2016**, *8*, 625–632.
[47] J. T. Foy, Q. Li, A. Goujon, J.-R. Colard-Itté, G. Fuks, E. Moulin, O. Schiffmann, D. Dattler, D. P. Funeriu, N. Giuseppone, *Nat. Nanotechnol.* **2017**, *12*, 540–545.
[48] M. Camacho-Lopez, H. Finkelmann, P. Palffy-Muhoray, M. Shelley, *Nat. Mater.* **2004**, *3*, 307–310.
[49] T. Ikeda, J. Mamiya, Y. Yu, *Angew. Chem. Int. Ed.* **2007**, *46*, 506–528.
[50] C. L. van Oosten, C. W. M. Bastiaansen, D. J. Broer, *Nat. Mater.* **2009**, *8*, 677–682.
[51] S. Iamsaard, S. J. Aßhoff, B. Matt, T. Kudernac, J. J. L. M. Cornelissen, S. P. Fletcher, N. Katsonis, *Nat. Chem.* **2014**, *6*, 229–235.
[52] T. J. White, D. J. Broer, *Nat. Mater.* **2015**, *14*, 1087–1098.
[53] A. H. Gelebart, D. J. Mulder, M. Varga, A. Konya, G. Vantomme, *Nature* **2017**, *546*, 632–636.
[54] S. J. Aßhoff, F. Lancia, S. Lamsaard, B. Matt, T. Kudernac, S. P. Fletcher, N. Katsonis, *Angew. Chem. Int. Ed.* **2017**, *56*, 3261–3265.
[55] F. K. C. Leung, T. van den Enk, T. Kajitani, J. Chen, M. C. A. Stuart, J. Kuipers, T. Fukushima, B. L. Feringa, *J. Am. Chem. Soc.* **2018**, *140*, 17724–17733.
[56] E. D. Sone, S. I. Stupp, *Chem. Mater.* **2011**, *23*, 2005–2007.

10.1002/anie.201905445

WILEY-VCH

COMMUNICATION

3D unidirectionally aligned responsive supramolecular hierarchical assemblies have much potential in biomedical materials and soft actuators. Macroscopic motor amphiphile strings, decorated with iron nanoparticles, provide fast response photoactuation and magnet induced movements that allows a systematic cargo transport process.

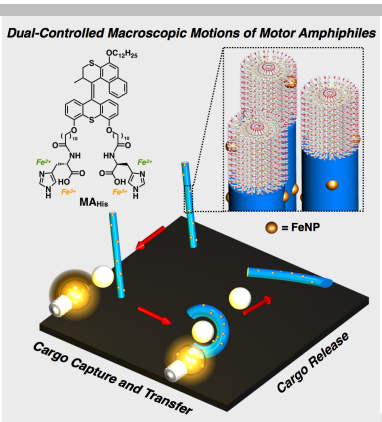

Dr. Franco King-Chi Leung, Dr. Takashi Kajitani, Dr. Marc C. A. Stuart, Prof. Dr. Takanori Fukushima, Prof. Dr. Ben L. Feringa**

Page No. – Page No.

Dual-Controlled Macroscopic Motions in A Supramolecular Hierarchical Assembly of Motor Amphiphiles